Organic & Biomolecular Chemistry

Julolidine-Based Small Molecular Probes for Fluorescence Imaging of RNA in Live Cells

Journal:	*Organic & Biomolecular Chemistry*
Manuscript ID	OB-ART-08-2023-001314.R1
Article Type:	Paper
Date Submitted by the Author:	24-Aug-2023
Complete List of Authors:	Mondal, Iswar; Indian Institute of Technology Mandi, School of Chemical Sciences Rawat, Priya; Indian Institute of Technology Mandi, School of Biosciences and Bioengineering Galkin, Maksym; Institute of Organic Chemistry and Biochemistry Czech Academy of Sciences Deka, Snata; Indian Institute of Technology Mandi, School of Chemical Sciences Karmakar, Anirban; Instituto Superior Técnico, Centro de Química Estrutural Mondal, Prosenjit; Indian Institute of Technology Mandi, School of Biosciences and Bioengineering Ghosh, Subrata; Indian Institute of Technology Mandi, School of Chemical Sciences

Julolidine-Based Small Molecular Probes for Fluorescence Imaging of RNA in Live Cells

Iswar Chandra Mondal,[a] Priya Rawat,[b] Maksym Galkin,[c] Snata Deka, [a] Anirban Karmakar,[d] Prosenjit Mondal, *[b] and Subrata Ghosh*[a]

a. *School of Chemical Science, Indian Institute of Technology Mandi, H.P-175005, India*
b. *School of Bio Sciences and Bioengineering, Indian Institute of Technology Mandi, H.P-175005, India*
c. *Laboratory of Chemical Biology, The Institute of Organic Chemistry and Biochemistry of the Czech Academy of Sciences, Prague 6 16610, Czech Republic*
d. *Centro de Química Estrutural, Instituto Superior Técnico, Avenida Rovisco Pais, 1049-001 Lisboa, Portugal*

Abstract

Intracellular RNA imaging with organic small molecular probes has been an intense topic, although the number of such reported dyes, particularly dyes with high quantum yield and long wavelength excitation/emission are quite limited. The present work reports the design and synthesis of three cationic julolidine-azolium conjugates (OX-JLD, BTZ-JLD and SEZ-JLD) as turn-on fluorescent probes with appreciably high quantum yields and brightness upon interaction with RNA. A structure-efficiency relationship has been established for their potential towards interaction and imaging of intracellular RNA. Given their chemical structure, the free rotation between donor and acceptor gets restricted when the probes bind with RNA resulting in strong fluorescence emission towards higher wavelength upon photoexcitation. A detailed investigation revealed that the photophysical properties and the optical responses of two probes, *viz* BTZ-JLD and SEZ-JLD, towards RNA, are very promising and qualify them to be suitable candidates for biological studies particularly for cellular imaging applications. The probes allow imaging of intracellular RNA with prominent staining of nucleoli in live cells under a range of physiological conditions. The results of the cellular digest test established the appreciable RNA-selectivity of BTZ-JLD and SEZ-JLD inside the cellular environment. Moreover, acomparison between the relative intensity profile of SEZ-JLD before and after the RNA-digestion test inside the cellular environment indicated that the interference of cellular viscosity in fluorescence enhancement is insignificant, and hence, SEZ-JLD can be used as cell membrane permeable cationic molecular probe for deep-red imaging of intracellular RNA with a good degree of selectivity.

Key Words: *styryl dye; molecular rotor; intracellular RNA imaging; fluorescence microscopy, deep red imaging.*

Introduction

As reported in the literature, molecular rotors have been recognized as utility tools for fluorescence imaging, allowing quantitative readouts of microenvironments inside the cells as well as specific biomolecular interactions.[1-3] Cyanine, hemicyanine and styryl dyes which have been widely used fluorescent probes possess typical donor-acceptor architecture separated with a π-rich spacer.[3-7] In general, these dyes undergo intramolecular twisting motion upon photoexcitation which further tunes the photoemission from such molecular systems.[3-7] This phenomenon has been widely explored to develop task-specific molecular rotors, particularly for fluorescence imaging.[8, 9] The remarkable popularity of cyanine dyes for biological applications is largely due to their high degree of selectivity, appreciable quantum yield with tunable optical properties, excitation/emission at longer wavelengths, good cell membrane permeability and many more.[10, 11]

In recent times, fluorescence imaging has been proven to be a highly efficient analytical tool in biomedical research mainly due to its high sensitivity, quick response time and high specificity.[12-16] This apart, fluorescence imaging is also becoming an emerging tool in many other important domains that include forensics,[17, 18] agriculture,[19, 20] textile,[20, 21] sensing[22] and so on. Considering the potential of this fascinating optical tool, a large, number of fluorescent probes have been designed and developed to make this technique successful for labelling biomolecules, sensing different ions, and visualization of a particular region of biological species.[23-28]

Dynamic tracking of cellular organelles is very important to get deep insights into different cellular processes involved in various biological events.[29-32] In this context, small molecular fluorescent probes targeting specific cellular organelles such as mitochondria, lysosomes, endoplasmic reticulum, nucleus, nucleolus etc. are highly promising due to their superior intracellular chemical tractability, good biocompatibility, and rich design ability with exciting photophysical properties.[33-38] Among several organelles, the nucleus is the central attraction of the eukaryotic cell, which contains almost all of the cell genome,[39-41] and nucleolus is the key site inside it for synthesizing and assembling of ribosomal RNAs.[42-44] It also controls cell growth and proliferation.[45] However, the details of the nucleolar dynamics, global dynamics of RNA distribution, and transcriptional activity are still under investigation.[46] The biological functions of the nucleus are not completely known yet as it is difficult to study the complete nucleolar dynamics in the prefixed cell.[29] Hence, live-cell imaging comes into the picture to understand and visualize all nucleus-related bio-event.[47]

Fluorescence in situ hybridization (FISH),[48] molecular beacons,[49] GFP-tagged RNA binding proteins,[50] denaturing gradient gel electrophoresis and DNA microarray techniques[51] are widely used to visualize the structure and function of rRNA.[52] However, these techniques cannot provide us with the spatiotemporal information of the three-dimensional structure of rRNA.[53] Quantum dots with surface functionalization have been explored to visualize the nucleus and nucleolus due to their high quantum yield and high photo-stability.[54, 55] Few metal complexes have been designed to label the nucleus and nucleolus.[56, 57] However, in most cases, either complex surface modification is needed, or the material suffers from poor cell permeability and cytotoxicity.

Hence low molecular weight organic probes get immense attraction for live-cell imaging,[58, 59] although such probes are relatively limited in number particularly for RNA imaging. In this regard, SYTO® RNA select is the only well-known commercial RNA imaging probe. To our knowledge, the chemical structure of this probe has not been disclosed yet. Hence, apart from intense academic importance, there is a strong industrial aspect of molecular RNA-specific fluorescent dyes.[60] Among the few interesting, reported probes, Turro and co-workers demonstrated one RNA selective FRET-base probe consisting of covalently linked fluorescein and EtBr.[61] The probe itself is fluorescent under visible light (488 nm) excitation in the absence of RNA. However, in the presence of RNA, it shows strong emission at 620 nm. Chang and Co-workers reported a library of stryl derivatives, which exhibited fluorescence in the red region (λ_{max} = 620 nm) upon binding with RNA.[62] A structurally modified bulky Hsd probe for RNA was reported by Peng group.[60] This probe requires host macrocyclic molecule for its functioning.[63] Similarly, a CP series of molecules was designed and reported by Wang et al.[64] Fisher and co-workers reported a styryl-quinolinium conjugate for the imaging of ribosomal RNA.[65] Recently, Cesaretti et. al reported far-red RNA-selective dyes for cellular imaging.[66] Moreover, a few emissive probes which emit in the blue[67] and green[68] regions of the electromagnetic spectrum have been reported in the literature.[69] Therefore, the need for developing RNA-specific small organic probes having promising characteristic features such as high quantum yield, good brightness, low cytotoxicity and so on for live-cell imaging is very evident.

Given the need and scope as described above, we report our recent efforts on the design and development of chalcogen based three cationic molecular rotors (OX-JLD, BTZ-JLD and SEZ-JLD) comprised of julolidine-azolium conjugate for fluorescence imaging of intracellular RNA including ribosomal RNA in the live cell. After investigating the optical properties of all the developed probes, BTZ-JLD and SEZ-JLD turned out to be the best ones for RNA recognition and imaging in the cellular environment. Hence, preliminary cellular-level studies were performed with these two probes. For comparative analysis, we performed a few control experiments with BTZ-JLD and SEZ-JLD. However, given its maximum red-shifted absorption and emission among the three, SEZ-JLD was selected and tested extensively for complete biological studies. Interestingly, SEZ-JLD itself is almost non-fluorescent and thus ensures no background fluorescence due to the emission from the probe itself during cellular imaging studies. In the presence of RNA, SEZ-JLD emits remarkably strong deep-red fluorescence. To mention a few of its good characteristics, SEZ-JLD showed low cytotoxicity, highly specific to cellular RNA over DNA as established from digest test, high quantum yield (~34%), good brightness, cell membrane permeability without any permeabilizing agent and a high degree of aqueous solubility. Moreover, its weak response toward fluorescence enhancement in moderate viscous medium as compared to the enhancement in the presence of RNA (established through lifetime measurements) also supported the insignificant interference of cellular viscosity-driven emission enhancement with the RNA-interaction-based fluorescence imaging.

Experimental Section

Materials

All commercial solvents and chemicals were obtained from Sigma Aldrich, TCI chemicals, Avra Synthesis and BLD Pharm, and utilized without additional purification. The human hepatocellular carcinoma HepG2 cell line (HB-8065), was procured from American Type Culture Collection. For photophysical experiments, spectroscopic grade dimethyl sulfoxide (DMSO) was utilized. Doubly deionized water from Milli-Q systems was utilized in all studies. Using doubly deionized water, PBS (pH = ~7.34, 0.01 M) was made. PBS was used to prepare DNA (Herring Sperm, Sigma Aldrich) and RNA (Torula yeast, Sigma Aldrich) solutions (1 mg/mL). Stock solutions (5 mM) of OX- JLD, BTZ-JLD and SEZ-JLD were prepared in DMSO. All photophysical studies were done using DMSO stock solutions.

Instruments

^{1}H and ^{13}C NMR spectra were recorded on a Jeol JNM ECX 500 MHz spectrometer. Bruker Maxis Impact HD device was used to record MS-ESI spectra. The absorption/emission spectra were acquired using a 1 cm quartz cell with 5/5 slit widths (1/1 for absorption) on a Shimadzu UV-2450 and a Horiba Fluorolog spectrophotometer, respectively. The photostability experiment was performed under a mercury vapour lamp. The Fluorescence Lifetime Spectrometer (Agilent technology) was used to measure lifetime. A Laser Scanning Confocal Microscope (Nikon Eclipse Ti confocal microscope) was used to carry out cell imaging investigations.

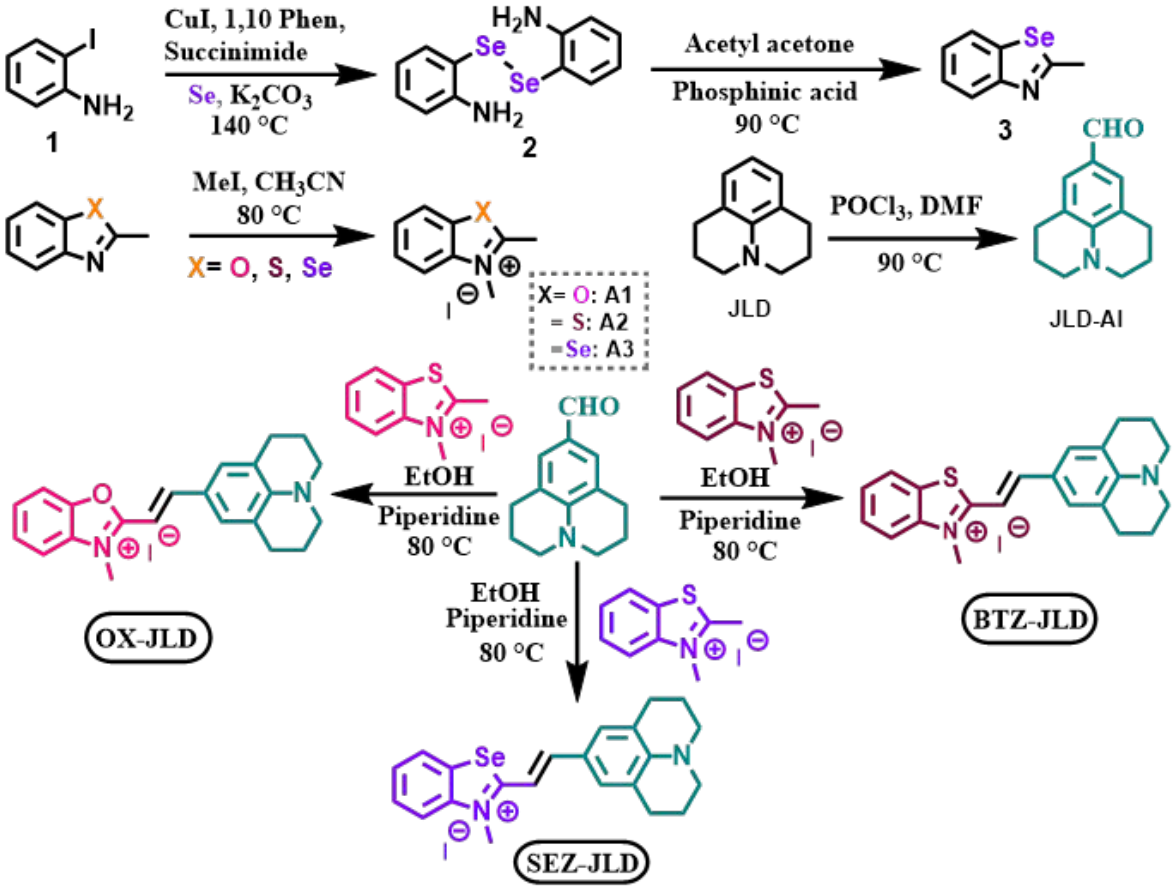

Scheme 1: Synthetic pathways for the probes OX-JLD, BTZ-JLD and SEZ-JLD.

Synthesis

General synthesis procedure

The probes were synthesized following a few-steps synthesis procedure as outlined in **Scheme-1**. 2-Methyl benzoxazole and 2-methyl benzothiazole were purchased from commercial sources. Initially, 2-methyl benzoazole iodide salts (A1, A2, A3), as well as julolidine aldehyde (JLD-Al), were prepared following literature reports[44, 70, 71] (for detailed procedure please check ESI). Finally, the iodide salts of respective 2,3-dimethyl benzo-azoles (1 eq) and julolidine aldehyde (1.2 eq) were dissolved in ethanol in a round bottom flask and refluxed for 12 hours. The solvent was removed under reduced pressure after completion of the reaction, and the solid was then triturated with ethyl acetate. Column chromatography was used to further purify the crude product using neutral alumina as the stationary phase and 1% methanol in DCM as eluent.

Compound OX-JLD [(E)-3-methyl-2-(2-(2,3,6,7-tetrahydro-1H, 5H-pyrido [3,2,1-ij] quinolin-9-yl) vinyl) benzo[d] oxazol-3-ium iodide]. Deep blue Solid; Yield: 75%; ^{1}H NMR (500 MHz, DMSO-d_6): 7.98 (d, J = 15.1 Hz, 1H), 7.84 (t, J = 7.6 Hz, 2H), 7.59 – 7.52 (m, 2H), 7.43 (s, 2H), 7.08 (d, J = 15.1 Hz, 1H), 3.96 (s, 3H), 3.33 – 3.30 (m, 4H), 2.67 (t, J = 6.2 Hz, 4H), 1.84 (p, J = 6.9 Hz, 4H). ppm. ^{13}C NMR (125 MHz, DMSO-d_6): 176.28, 163.46, 151.34, 148.62, 147.28, 132.11, 127.65, 127.33, 121.68, 120.62, 113.55, 112.17, 94.51, 50.20, 32.01, 27.49, 21.10 ppm; MS: m/z calculated for $C_{22}H_{23}N_2O$ $[M-I]^+$ 331.1804, found 331.1804, Mass Error 0.00 ppm.

Compound BTZ-JLD [(E)-3-methyl-2-(2-(2,3,6,7-tetrahydro-1H, 5H-pyrido [3,2,1-ij] quinolin-9-yl) vinyl) benzo[d] thiazol-3-ium iodide]. Deep blue Solid; Yield: 85%; ^{1}H NMR (500 MHz, DMSO-d_6): δ = 8.23 (d, J = 7.2 Hz, 1H), 8.00 (d, J = 8.4 Hz, 1H), 7.85 (d, J = 14.9 Hz, 1H), 7.72 (ddd, J = 8.5, 7.3, 1.2 Hz, 1H), 7.64 – 7.59 (m, 1H), 7.49 (s, 2H), 7.42 (d, J = 15.0 Hz, 1H), 4.14 (s, 3H), 3.37 (s, 5H), 2.71 (t, J = 6.2 Hz, 4H), 1.89 (q, J = 6.0 Hz, 4H). ppm. ^{13}C NMR (125 MHz, DMSO-d_6): 170.82, 150.59, 148.31, 142.45, 130.97, 129.18, 127.49, 126.93, 124.17, 121.67, 121.08, 115.98, 104.70, 50.18, 35.75, 27.46, 21.10 ppm; MS: m/z calculated for $C_{22}H_{23}N_2S$ $[M-I]^+$ 347.1576, found 347.1575, Mass Error 0.28 ppm.

Compound SEZ-JLD [(E)-3-methyl-2-(2-(2,3,6,7-tetrahydro-1H,5H-pyrido [3,2,1-ij] quinolin-9-yl)vinyl) benzo[d][1,3] selenazol-3-ium iodide]. Deep blue Solid; Yield: 85%; ^{1}H NMR (500 MHz, DMSO-d_6): δ 8.28 (d, J = 9.3 Hz, 1H), 7.95 (d, J = 7.2 Hz, 1H), 7.90 (d, J = 14.7 Hz, 1H), 7.70 – 7.66 (m, 1H), 7.56 – 7.50 (m, 3H), 7.47 (d, J = 14.8 Hz, 1H), 4.12 (s, 3H), 3.37 (t, J = 5.8 Hz, 4H), 2.73 (t, J = 6.3 Hz, 4H), 1.93 – 1.87 (m, 4H) ppm. ^{13}C NMR (125 MHz, DMSO-d_6): δ 178.14, 152.74, 148.54, 143.90, 131.25, 128.85, 127.84, 127.26, 127.22, 121.78, 121.63, 117.37, 107.76, 50.28, 36.87, 27.45, 21.14 ppm; MS: m/z calculated for $C_{22}H_{23}N_2Se$ $[M-I]^+$ 395.1028, found 395.1026, Mass Error 0.50 ppm.

Fluorescence Lifetime

Lifetime measurements were performed using 2.5 μM of probe in PBS (pH=7.34, 0.01M) containing 1 mg/mL RNA. The excited state dynamics were assessed utilizing a Fluorescence Lifetime Spectrometer (Agilent technology) with a 574 nm light emitting diode (LED). It should be emphasized that the probe alone (SEZ-JLD)

is almost non-fluorescent, therefore we were unable to determine its lifetime. Hence, we contrasted the lifetime with the industry-standard control (LUDOX® TM-50) for comparison. Lifetime measurement of SEZ-JLD in Glycerol-Water mixture was done using a 574 nm light emitting diode as the excitation source.

Cell Imaging

HepG2 cells were seeded onto a chamber slide. Next day, cells were treated with 5 μm BTZ-JLD and SEZ-JLD for 20 min and incubated at 37 °C incubator at 5% CO_2. After treatment, cells were fixed with 4% PFA for 10 min and then the cells were washed three times with PBS (5 min each) and then finally, the cells were mounted using DAPI mounting media (Vectorshield #Cat H1200) and observed using Nikon Eclipse Ti confocal microscopy.

RNase digest test

Cells were initially fixed with 4% paraformaldehyde for one hour at room temperature. The cells were then submerged in 1% Triton X-100 for 5 minutes to permeabilize through the cell membrane. Following two PBS rinses, 200 μL of clean PBS was added in two wells (as a control experiment), followed by the addition of 50 μg/mL DNase-free RNase A (QIAGEN) in 200 μL PBS. The wells were then incubated at 37 °C in 5% CO_2 for two hours. Following a PBS wash, the cells were treated with RNase and a 5 μM solution of BTZ-JLD and SEZ-JLD was added to the control. Next, the cells were kept in a 5% CO_2 environment for 1 hour at 37 °C. Cells were twice rinsed with clean PBS before imaging. Imaging was performed on Nikon Eclipse Ti confocal microscope at 60× objective.

Cytotoxicity assay

Cytotoxicity of SEZ-JLD was analysed by MTT assay. Briefly, 10000 cells were seeded in a 96-well plate in 100 μl DMEM supplemented with FBS and PEN-STREP. After overnight incubation, cells were treated with SEZ-JLD (1, 2.5, 5, 7.5 and 10 μM) for 24 hrs.10 μl of MTT (3-(4, 5-dimethyl thiazol-2yl)-2, 5-diphenyl tetrazolium bromide, 5 mg/ml prepared in PBS) was added per well and kept for 4hrs of incubation at 37℃. Formazan crystals were dissolved in 200 μl DMSO. Absorbance was measured at 570 nm using INFINITE 200 PRO microplate reader from Tecan. Cell viability was expressed as percent cell viability relative to control values and plotted using GRAPH PAD PRISM. The dose response viability was then used to calculate LD_{50} of SEZ-JLD for HepG2 cells using Graph Pad Prism5.

Results and Discussion

Design and Synthesis of Probes

Given that organochalcogen functionality may improve the optical properties of a chemical species,[72] and considering the known promising emissive nature of the julolidine unit, we designed three cationic molecular probes by integrating benzo-azolium unit with julolidine functionality (**Scheme 1**). The probes were synthesized

following the processes as outlined in **Scheme-1**. Thus, strong push-pull scaffolds were developed through the integration of the sturdy electron-donating julolidine and the electron-withdrawing cationic benzo-azole moiety, which are separated by a π-spacer. Due to the natural cationic activity, we predicted that this would aid in (i) extending the wavelength of absorption and emission, (ii) enhancing water solubility, and (iii) specifically targeting sub-cellular areas like the nucleolus. Additionally, it has been reported that adding chalcogen atoms to molecular scaffolds is a great way to develop emissive molecular probes with enhanced optical characteristics.[73] The detailed synthetic procedures and characterization of probes and the intermediates are given in the experimental section and in the ESI.

Single Crystal Structure Analysis

We were successful in growingdark purple single crystals of SEZ-JLD from a DCM-methanol mixture (1:1) by using the slow evaporation method. The structural analysis of SEZ-JLD demonstrates that its asymmetric unit contains two cationic SEZ-JLD molecules and two anionic iodine counter ions. In this molecule, the methyl benzoselenazole ring and the julolidine ring are present almost in the same plane, thus the overall geometry of SEZ-JLD is planner (Figure 1A). However, the -CH_2 groups in the julolidine ring remain slightly (0.32-0.73 Å) outwards from the molecular plane. The ball and stick structure and packing diagram of the SEZ-JLD are presented in Figure 1. In SEZ-JLD, we have observed various types of non-covalent interactions, for example, the anionic iodines act as trifurcated acceptors and established various weak C-H···I interactions [d_{H-A} 3.103-3.164 Å] with aromatic-CH and methyl-CH groups. Besides that, we have also observed very weak non-covalent interaction between the Se atom and aromatic -CH group [d_{D-A} 3.710 Å; <D–H····A 127˚]. In SEZ-JLD, various C-H····π interactions, having $d_{H-\pi}$ distances in the range of 2.585-2.843 Å, between the CH_2 groups of the julolidine and the benzoselenazole ring were observed.

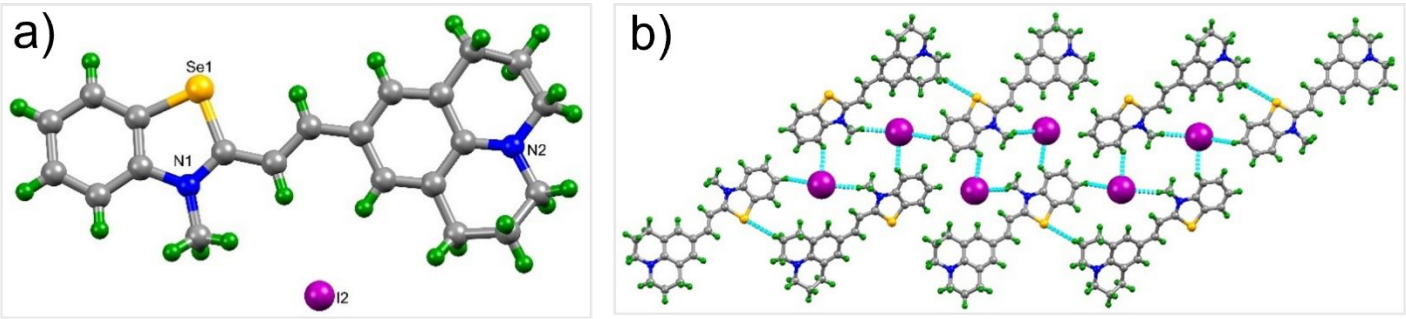

Figure 1: a) The ball and stick representation of SEZ-JLD. b) The hydrogen bonded packing diagram of SEZ-JLD (the iodine molecules are represented in a space-fill model).

Optical Properties

To investigate the impact of solvent polarity on the optical response of OX-JLD, BTZ-JLD, and SEZ-JLD, the absorption and emission spectra were recorded in a variety of solvents. The absorption maxima of the probes got blue-shifted and displayed a uniform pattern with increasing solvent polarity (**Figure S1, S3, S5** and **Table S1**).

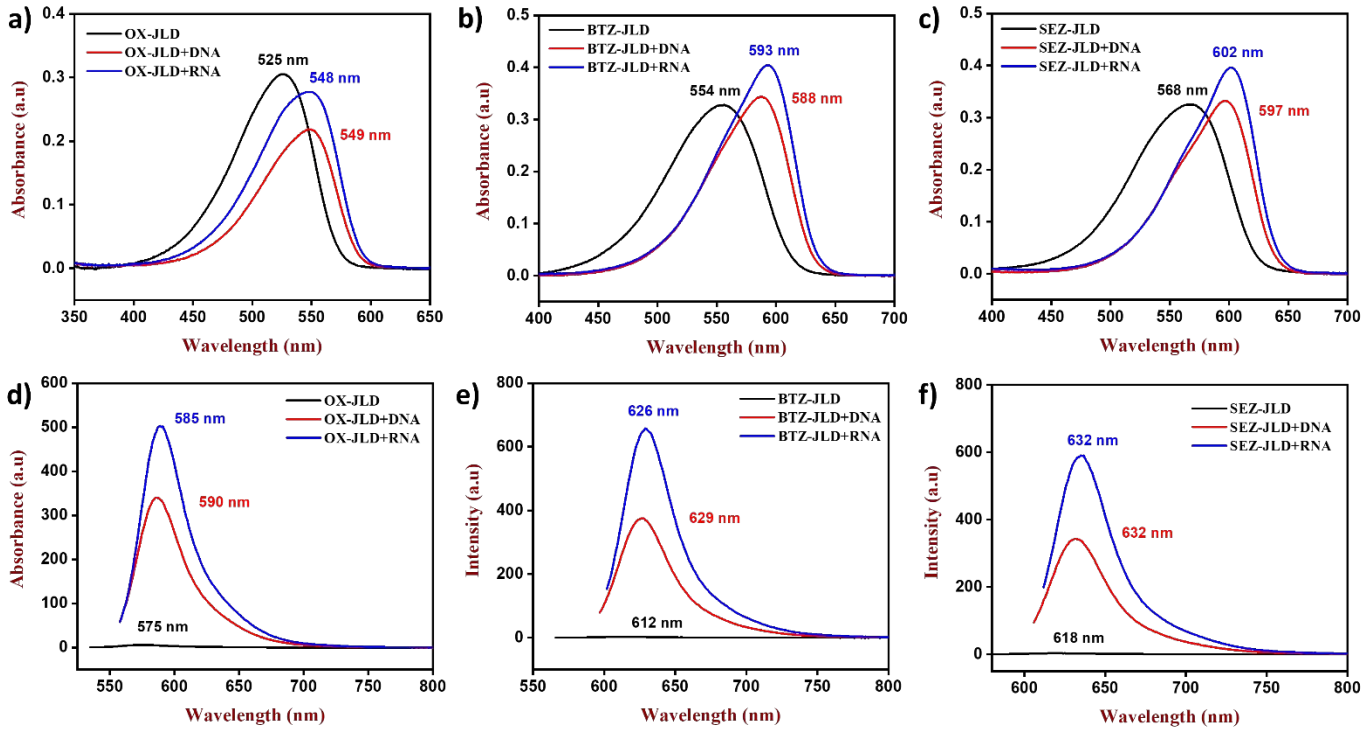

Figure 2: Absorption and emission spectra at fixed concentration (2.5 μM) of respective dyes in the presence of DNA and RNA (absorption and emission maxima values are indicated in each figure).

Due to the ground state stabilization in a polar environment and a reduction in the excited state's dipole moment, styryl dyes develop their distinctive negative solvatochromic behaviour.[74] However, relatively much lesser changes in the emission maxima in different solvents were observed (**Figure S2, S4, S6** and **Table S1**). The probe OX-JLD and BTZ-JLD absorb light at the lower wavelength side of the electromagnetic spectrum (525 nm and 554 nm) as compared to SEZ-JLD (568 nm) (**Figure 2a** and **2b**). In the presence of DNA and RNA, the absorption maxima of all the probes got shifted to longer wavelengths (Figures **2a** and **2b**). Interestingly, all three probes were found to be almost optically silent ($\phi_{OX\text{-}JLD}$ **=0.0041**, $\phi_{BTZ\text{-}JLD}$ **=0.0019,** $\phi_{SEZ\text{-}JLD}$ **=0.007**), however, a drastic change in fluorescence intensity was observed in the presence of nucleic acids (**Figure 2d**, **2e**, **2f**, and **Table S4**). OX-JLD, BTZ-JLD and SEZ-JLD showed emission maxima at 590 nm, 629 nm, and 632 nm respectively, in the presence of RNA. When treated with DNA, the probes OX-JLD, BTZ-JLD and SEZ-JLD also showed fluorescence enhancement with emission maxima at 585 nm, 626 nm and 632 nm respectively. Hence, a careful review of the absorption and emission properties of OX-JLD, BTZ-JLD and SEZ-JLD revealed that SEZ-JLD showed the maximum red-shifted absorption and emission maxima in the presence of nucleic acids (**Figure 2a-e**). As the stock solutions of the present probes were prepared in DMSO, it was very important to check if the probes undergo any aggregation when it is present in higher concentration in the stock solution. This event was studied using the stock solution of SEZ-JLD. To complete the study, the stock solutions of different concentrations in DMSO were prepared, and their absorption spectra were measured. Interestingly, a linear relationship between absorbance and concentration was observed in the concentration range of 5–20 μM (**Fig. S9**). These results

indicated that possibly there was no aggregation of SEZ-JLD even at higher concentrations in DMSO. Next, the quantum yields of all three probes in the presence of RNA were calculated and found to be 0.41, 0.43, and 0.37 for OX-JLD, BTZ-JLD and SEZ-JLD, respectively (**Table S4**). As the quantum yields of these probes were comparable and, as SEZ-JLD showed maximum red-shifted absorption and emission in the presence of RNA, we chose SEZ-JLD as the model probe for more detailed studies.

Notably, in the presence of RNA, SEZ-JLD (2.5 μM) showed an approximately 256 folds enhancement in the fluorescence intensity with emission maxima of 635 nm (**Figure 2f**) when excited at 602 nm. Similarly, the probe exhibited strong fluorescence in the presence of DNA with emission maxima of 630 nm when excited at 600 nm. Given that the developed probes have molecular rotor-type chemical architecture.[75] It was very important to study the effect of solvent viscosity on the emission property of these probes. To investigate this, we chose the water-glycerol experiment as one of the most commonly used techniques to study the effect of viscosity. As observed, an increase in viscosity (20% glycerol in water to 100% glycerol) led to an enhancement of ~23-fold (at 625 nm) in fluorescence intensity in the absence of any nucleic acid in the solution (**Figure 3a**). This increase in intensity is ascribed to the molecular rotations being constrained in the highly viscous glycerol, which prevents optical losses to a greater extent through non-radiative routes. As expected, an increase in the fluorescence lifetime of SEZ-JLD with the increase in glycerol content in the water-glycerol mixture was observed (0.5 ns in glycerol). This in turn established the impact of medium viscosity in enhancing the fluorescence intensity of SEZ-JLD (**Figure 3b**). However, such viscosity-driven fluorescence lifetime enhancement was not very significant as compared to the lifetime of SEZ-JLD in the presence of RNA (2.26 ns) (**Figure 3d** and **Table S2**). Hence, as presented in **Figure 3c**, in terms of lifetime enhancement, although the higher viscosity of the medium induced good fluorescence emission with an increase in fluorescence lifetime, the presence of RNA brought in a drastic enhancement in fluorescence emission with a high lifetime which is almost five times of the lifetime of SEZ-JLD in glycerol. These results concluded that SEZ-JLD has a strong affinity toward RNA leading to strong enhancement in fluorescence emission as well as in lifetime, and thus the interference of viscosity-induced fluorescence emission may not be significant for further studies. Thus, the lighting-up of non-fluorescent SEZ-JLD in the presence of RNA indicated its possible use for cellular imaging applications as the background fluorescence issue is suppressed due to the non-fluorescent nature of SEJ-JLD. Also, as the optical properties of BTZ-JLD were similar to that of SEZ-JLD, it was also selected for preliminary cellular studies. However, given the shorter wavelength emission of OX-JLD, it was not chosen for further studies.

It seems a non-radiative twisted intramolecular charge transfer (TICT) state is formed when julolidine and benzoselenazole units freely rotate in a non-viscous or low viscous environment upon photoexcitation and thus produce extremely faint fluorescence emission.[76] However, the creation of the TICT state is hampered when the rotation is constrained, and thus strong fluorescence is produced in an environment with high viscosity.[3, 76] When titrating against an increasing concentration of DNA and RNA, a progressive increase in fluorescence intensity was seen (**Figure S10-11**). Up to 100 μg/mL, there was a linear relationship between the change in fluorescence

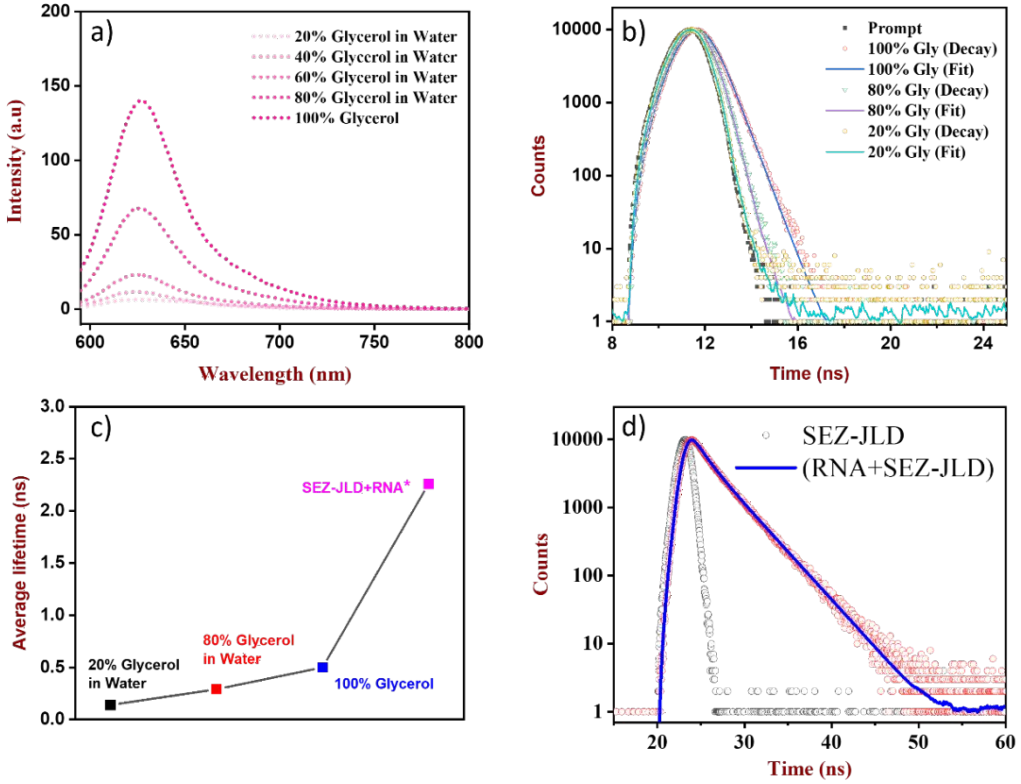

Figure 3: a) Emission spectra of SEZ-JLD in glycerol/water mixtures; b) Variation in lifetime at different percentage of glycerol; c) Comparison of average lifetimes of the probe in glycerol mixture and with RNA; d) Fluorescence lifetime measurement of SEZ-JLD in the presence of RNA (1mg/mL).

intensity and the concentration of nucleic acid, which corresponds well with the sigmoidal equation (**Figure S12**). As observed, the fluorescence intensity of SEZ-JLD was increased by more than 10% even in the presence of 0.75 µg/mL RNA (**Figure S13**). This indicates that SEZ-JLD can detect RNA at very low concentrations. Also, SEZ-JLD showed ~48 times enhancement in quantum yield in the presence of RNA (ϕ_{RNA}=0.34, relative to Rhodamine B) as compared to SEZ-JLD alone (ϕ_{PBS}=0.007, relative to Rhodamine B) (**Table S3**). Given the almost non-fluorescent nature of SEZ-JLD (**Table S5**) and a strong enhancement in fluorescence signal with ~48 times enhancement in quantum yield in the presence of RNA and longer wavelength excitation/emission, it could be concluded that cellular imaging with SEZ-JLD can be done with almost no autofluorescence or background fluorescence. Similarly, ~226 times increase in quantum was observed when BTZ-JLD was treated with RNA (**Table S4**).

Next, as SEZ-JLD was chosen from the pool of three developed probes for all further studies mainly due to its highest red-shifted emission, its affinity for other typical biomolecules was examined. Other than nucleic acids, SEZ-JLD displayed very weak or no affinity toward many other analytes including proteins, enzymes, and small molecules (**Figure S14**). Also, we calculated the sensitivity of the probe SEZ-JLD towards RNA in the presence of such common biomolecules which shows its applicability in complex cellular environments (**Figure S15-19**). Furthermore, we investigated how the pH range (4–10) affected the probe's emission profile. We observed a good enhancement in emission intensity in the mentioned pH range (**Figure S20**).

Cellular Imaging

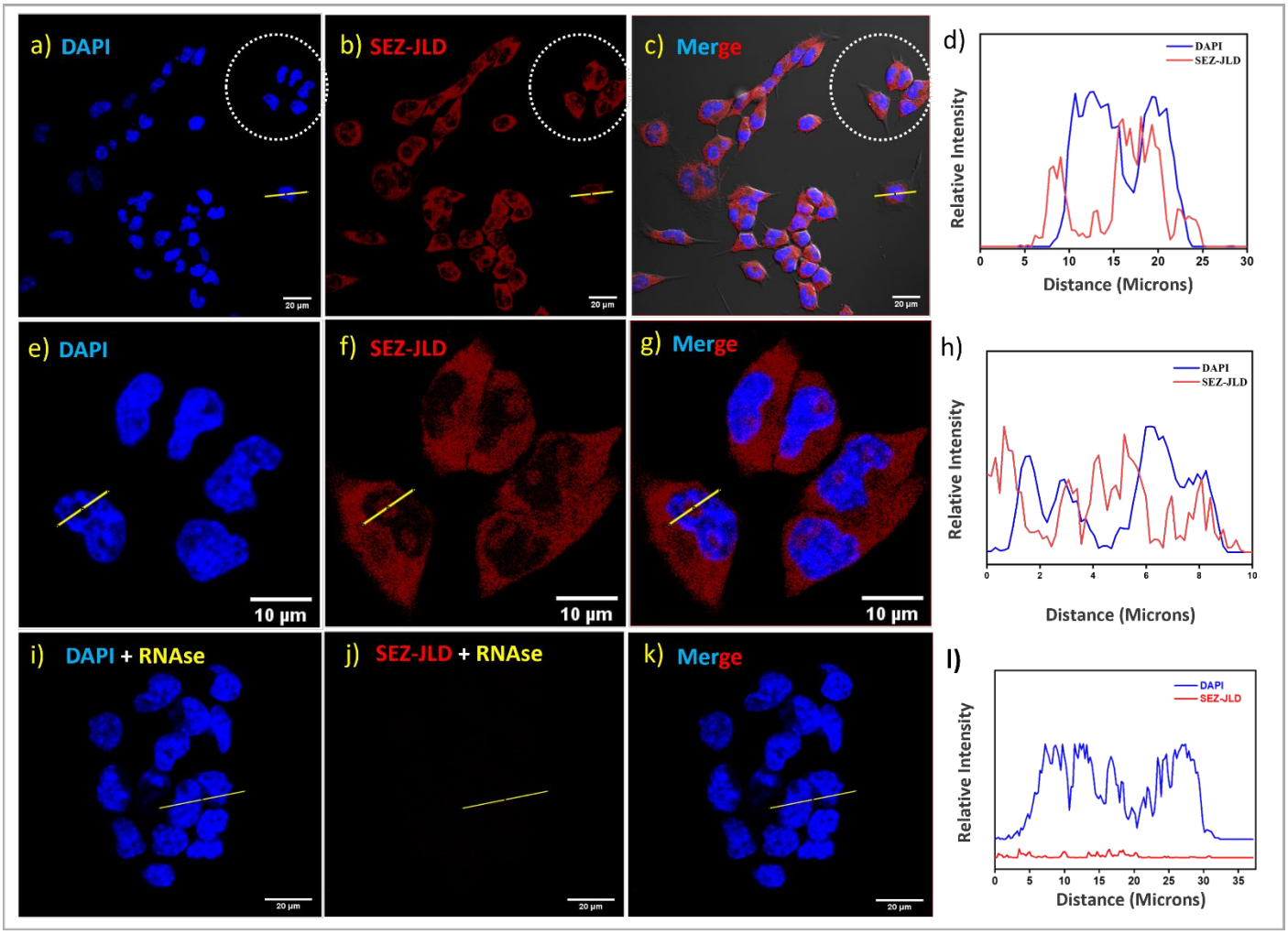

Figure 4: Localization of the compounds in live HepG2 cells: a) DAPI, b) SEZ-JLD, c) overlay of a) and b) images, and d) Intensity profile of c) image at ROI. Localization of the compounds in live HepG2 cells at higher magnification: e) DAPI f) SEZ-JLD g) overlay of e) and f) images, and h) intensity profile of g) image at ROI. RNase digest test of the probe: i, j) RNase treated cells stained with DAPI and SEZ-JLD, respectively. k) Overlay of i) and j) images. l) Intensity profile of k) image at ROI. The concentration of the probe is fixed to 5 µM for all imaging purpose; λ_{ex} = 561 nm and emission filter 570-620 nm were set to visualize SEZ-JLD. λ_{ex} = 405 nm and emission filter 425-475 nm were set to visualize DAPI.

Considering the promising optical properties and the results of solution phase studies, we became curious to investigate the potential of BTZ-JLD and SEZ-JLD as cellular imaging dyes. To our surprise, treatment of HepG2 cells for 30 min at 37 °C with 5 µM SEZ-JLD and BTZ-JLD solutions in PBS resulted in bright imaging of intracellular RNA (**Figure 4b** and **S21**). It is to be noted that both probes did not require a permeabilization agent to penetrate the cell membrane. A colocalization experiment was conducted using DAPI. The spotted intense areas are most likely the nucleoli of the cells, where ribosomal RNAs are synthesized (**Figure 4a-c**). The fact that the probes may stain both, nucleolus and cytoplasmic RNA in live cells, was evident from the significant fluorescence emission of these probes in the cytoplasmic region around the nucleus (**Figure 4a-c** and **S21a-c**). To prove further, RNA digestion test was done to validate RNA selective staining. Drastic reduction in

intracellular fluorescence emission indicated that SEZ-JLD stained intracellular RNA in live cells (**Figure 4e-g**). However, BTZ-JLD was found to be relatively less selective as significant emission was observed even after the digestion test (**Figure S21d-f**). As SEZ-JLD was found to be more promising for cellular studies considering its selectivity, it was further chosen for additional studies.

As SEZ-JLD acts as a molecular rotor, some extent of fluorescence emission from the cytoplasm area in the presence of SEZ-JLD was possibly due to freezing of rotation between donor and acceptor in the cytoplasm due to relatively higher viscosity in the cytoplasmic area and thus originating emission from local excited state (LE).[77-79] The extremely faint emission in the cytoplasmic region after the digest test further supported this conclusion.[80] However, as the cytoplasmic viscosity is not very high as compared to water,[81] strong emission due to viscosity difference cannot be expected. Therefore, the interference of cytoplasm viscosity toward cellular RNA imaging is almost insignificant. This is quite evident when we compared the relative intensity of SEZ-JLD before (**Figure 4d**) and after (**Figure 4h**) digestion test inside the cellular environment. It seems SEZ-JLD interacted more easily with the intracellular decondensed RNA than with highly condensed DNA, and this could be the origin of cellular RNA selectivity of SEZ-JLD over DNA. For any probe to be used for biological application, evaluation of the cytotoxicity of the probe is very important. When we investigated the cytotoxicity of SEZ-JLD using MTT assay, we observed that the probe is compatible with the cellular system with low cytotoxicity. It showed <30% cell death even after 24 hours while the cells were treated with 5 μM probe solution (**Figure S22**). Next, we investigated the photostability of SEZ-JLD in the solution phase. The probe demonstrated good photostability for 1 hour while illuminated with a mercury vapor lamp (165 W, 2.1 103 Lux) (**Fig. S23**). Good cell permeability, intense imaging, and good selectivity towards cellular RNA over DNA established SEZ-JLD as a potential emissive dye for long-term RNA trafficking.

Conclusion

To conclude, the present manuscript demonstrates the utilization of three julolidine-integrated organochalcogen-based cationic molecular platforms (SEZ-JLD, BTZ-JLD and OX-JLD) for intracellular imaging of RNA. The probes, BTZ-JLD and SEZ-JLD have excitation in the orange region and emission in the red region of the electromagnetic spectrum in the presence of RNA, while OX-JLD showed emission in the green region under similar conditions. During solution phase studies, these probes turned out to be highly sensitive toward RNA. Given its highest red-shifted emission among the three, SEZ-JLD was chosen as the model probe for many additional as well as cellular studies. It showed a practical detection of as low as 0.75 μg/mL of RNA. Although the water-glycerol mixture-based solution phase studies suggested that SEZ-JLD could induce fluorescence emission in a viscous medium, a systematic study through fluorescence lifetime measurements of SEZ-JLD in water-glycerol systems with varied water-to-glycerol ratios established that the lifetime even in pure glycerol (~0.5 ns, highest viscous medium in the present study) was approximately five times lower than the lifetime in the presence of RNA (~2.5 ns). These results indicated that SEZ-JLD has a very strong affinity toward RNA as

well as the interference of viscosity will be insignificant if cellular imaging studies are performed with SEZ-JLD. Also, it showed low cytotoxicity with only ~30% cell death even after 24 hours of treatment at working concentration. The most important characteristics of SEZ-JLD are its high quantum yield (~34%) and brightness of ~9000 $M^{-1}cm^{-1}$ which are the two highly desirable parameters for cellular imaging. Moreover, cellular imaging studies indicated that SEZ-JLD does not require any permeabilizing agent and it efficiently stains intracellular RNA within 30 minutes of incubation. The selectivity for RNA over DNA was established through the RNA digest test. The digest test also indicated that the interference of cellular viscosity toward fluorescence enhancement was insignificant. Together, we report a new organoselenium-based cell membrane permeable cationic molecular probe SEZ-JLD with impressive optical properties for deep red imaging of intracellular RNA.

Author Contribution

The manuscript is written through the contributions of all authors. All authors approved the final version of the manuscript.

Notes: The authors declare no competing financial interest.

Acknowledgement

Thanks to Advanced Materials Research Centre (AMRC), IIT Mandi, for its sophisticated instrumentation facility. I.C.M thankfully acknowledge the Ministry of Education, India for the research fellowship. A. K. expresses his gratitude to Instituto Superior Tecnico and FCT for a scientific employment contract (Contract No. IST-ID/107/2018) under Decree-Law No. 57/2016, of August 29.

References

1. W. L. Goh, M. Y. Lee, T. L. Joseph, S. T. Quah, C. J. Brown, C. Verma, S. Brenner, F. J. Ghadessy and Y. N. Teo, *Journal of the American Chemical Society*, 2014, **136**, 6159-6162.
2. J. Michl and E. C. H. Sykes, *ACS Nano*, 2009, **3**, 1042-1048.
3. M. A. Haidekker and E. A. Theodorakis, *Journal of Biological Engineering*, 2010, **4**, 11.
4. C. S. Abeywickrama, *Chemical Communications*, 2022, **58**, 9855-9869.
5. Y. Niko and A. S. Klymchenko, *The Journal of Biochemistry*, 2021, **170**, 163-174.
6. L. Yang, S. Chen, D. Yi, Q. Chen, J. Zhang, Y. Xie and H. Sun, *J Mater Chem B*, 2021, **9**, 8512-8517.
7. H.-W. Cao, X.-X. Lang, Y.-S. Chen, H.-W. Chen, J.-Z. Li, X.-F. Yu, H.-J. Wang and M.-Q. Wang, *Dyes and Pigments*, 2023, **210**, 111029.
8. J. Karpenko, Y. Niko, V. P. Yakubovskyi, A. O. Gerasov, D. Bonnet, Y. P. Kovtun and A. S. Klymchenko, *J Mater Chem C*, 2016, **4**, 3002-3009.
9. X. Luo, J. Li, J. Zhao, L. Gu, X. Qian and Y. Yang, *Chinese Chemical Letters*, 2019, **30**, 839-846.
10. G. S. Gopika, P. M. H. Prasad, A. G. Lekshmi, S. Lekshmypriya, S. Sreesaila, C. Arunima, M. S. Kumar, A. Anil, A. Sreekumar and Z. S. Pillai, *Materials Today: Proceedings*, 2021, **46**, 3102-3108.
11. X. Ma, L. Shi, B. Zhang, L. Liu, Y. Fu and X. Zhang, *Analytical and Bioanalytical Chemistry*, 2022, **414**, 4551-4573.
12. F. Hu and B. Liu, *Org Biomol Chem*, 2016, **14**, 9931-9944.
13. X. Li, X. Liang, J. Yin and W. Lin, *Chem Soc Rev*, 2021, **50**, 102-119.

14. X. Qian and Z. Xu, *Chem Soc Rev*, 2015, **44**, 4487-4493.
15. M. Schäferling, *Angewandte Chemie International Edition*, 2012, **51**, 3532-3554.
16. H. Zhang, X. Zhu, H. Li, G. Liu, J. Wang, A. Wang, L. Kong, W. Zhu and H. Zhou, *Anal Chem*, 2019, **91**, 14911-14919.
17. M. Wang, M. Li, A. Yu, Y. Zhu, M. Yang and C. Mao, *Advanced Functional Materials*, 2017, **27**, 1606243.
18. Y.-H. Chen, S.-Y. Kuo, W.-K. Tsai, C.-S. Ke, C.-H. Liao, C.-P. Chen, Y.-T. Wang, H.-W. Chen and Y.-H. Chan, *Anal Chem*, 2016, **88**, 11616-11623.
19. R. Zhang, Y. Ying, X. Rao and J. Li, *Journal of the Science of Food and Agriculture*, 2012, **92**, 2397-2408.
20. I. S. Marae, W. Sharmoukh, E. A. Bakhite, O. S. Moustafa, M. S. Abbady and H. E. Emam, *Cellulose*, 2021, **28**, 5937-5956.
21. W. Nie, J. Wu, J. Yang and L. Hu, *ACS Sustainable Chemistry & Engineering*, 2023, **11**, 3873-3881.
22. X. Wu, F. Tian, W. Wang, J. Chen, M. Wu and J. X. Zhao, *J Mater Chem C*, 2013, **1**, 4676-4684.
23. A. P. de Silva, H. Q. N. Gunaratne, T. Gunnlaugsson, A. J. M. Huxley, C. P. McCoy, J. T. Rademacher and T. E. Rice, *Chemical Reviews*, 1997, **97**, 1515-1566.
24. T. Terai and T. Nagano, *Curr Opin Chem Biol*, 2008, **12**, 515-521.
25. I. Johnson, *Histochem J*, 1998, **30**, 123-140.
26. F. Leblond, S. C. Davis, P. A. Valdes and B. W. Pogue, *J Photoch Photobio B*, 2010, **98**, 77-94.
27. M. Sameiro and T. Goncalves, *Chemical Reviews*, 2009, **109**, 190-212.
28. H. Zhu, J. L. Fan, J. J. Du and X. J. Peng, *Accounts of Chemical Research*, 2016, **49**, 2115-2126.
29. G. C. Yu, G. P. Tang and F. H. Huang, *J Mater Chem C*, 2014, **2**, 6609-6617.
30. H. Zhang, X. Zhu, G. Liu, X. Ding, J. Wang, M. Yang, R. Zhang, Z. Zhang, Y. Tian and H. Zhou, *Anal Chem*, 2019, **91**, 6730-6737.
31. Z. Lv, Z. Man, H. Cui, Z. Xu, H. Cao, S. Li, Q. Liao, Q. He, L. Zheng and H. Fu, *Advanced Functional Materials*, 2021, **31**, 2009329.
32. H.-R. Jia, Y.-X. Zhu, K.-F. Xu, G.-Y. Pan, X. Liu, Y. Qiao and F.-G. Wu, *Chemical Science*, 2019, **10**, 4062-4068.
33. X. Liu, Y. M. Sun, Y. H. Zhang, F. Miao, G. C. Wang, H. S. Zhao, X. Q. Yu, H. Liu and W. Y. Wong, *Org Biomol Chem*, 2011, **9**, 3615-3618.
34. Q. Li, Y. Kim, J. Namm, A. Kulkarni, G. R. Rosania, Y. H. Ahn and Y. T. Chang, *Chem Biol*, 2006, **13**, 615-623.
35. H. Li, Y. C. Li, H. H. Zhang, G. Y. Xu, Y. L. Zhang, X. H. Liu, H. P. Zhou, X. Y. Yang, X. J. Zhang and Y. P. Tian, *Chemical Communications*, 2017, **53**, 13245-13248.
36. W. Xu, Z. Zeng, J.-H. Jiang, Y.-T. Chang and L. Yuan, *Angewandte Chemie International Edition*, 2016, **55**, 13658-13699.
37. J. Lin, K. Yang and E. J. New, *Org Biomol Chem*, 2021, **19**, 9339-9357.
38. J. Yin, L. Huang, L. Wu, J. Li, T. D. James and W. Lin, *Chem Soc Rev*, 2021, **50**, 12098-12150.
39. J. S. Andersen, Y. W. Lam, A. K. L. Leung, S.-E. Ong, C. E. Lyon, A. I. Lamond and M. Mann, *Nature*, 2005, **433**, 77-83.
40. T. Misteli, *Cell*, 2004, **119**, 153-156.
41. C. S. Abeywickrama, K. J. Wijesinghe, C. B. Plescia, L. S. Fisher, T. Goodson, R. V. Stahelin and Y. Pang, *Photochemical & Photobiological Sciences*, 2020, **19**, 1152-1159.
42. M. M. Yusupov, G. Z. Yusupova, A. Baucom, K. Lieberman, T. N. Earnest, J. H. D. Cate and H. F. Noller, *Science*, 2001, **292**, 883-896.
43. V. Sirri, S. Urcuqui-Inchima, P. Roussel and D. Hernandez-Verdun, *Histochemistry and Cell Biology*, 2008, **129**, 13-31.
44. I. C. Mondal, M. Galkin, S. Sharma, N. A. Murugan, D. A. Yushchenko, K. Girdhar, A. Karmakar, P. Mondal, P. Gaur and S. Ghosh, *Chemistry – An Asian Journal*, 2022, **17**, e202101281.
45. Y. W. Lam, L. Trinkle-Mulcahy and A. I. Lamond, *J Cell Sci*, 2005, **118**, 1335-1337.
46. A. K. L. Leung, J. S. Andersen, M. Mann and A. I. Lamond, *Biochem J*, 2003, **376**, 553-569.
47. L. S. Forero-Quintero, W. Raymond, T. Handa, M. N. Saxton, T. Morisaki, H. Kimura, E. Bertrand, B. Munsky and T. J. Stasevich, *Nature Communications*, 2021, **12**, 3158.
48. J. J. L. Goh, N. Chou, W. Y. Seow, N. Ha, C. P. P. Cheng, Y.-C. Chang, Z. W. Zhao and K. H. Chen, *Nature Methods*, 2020, **17**, 689-693.
49. Y. Q. Xia, R. L. Zhang, Z. L. Wang, J. Tian and X. Y. Chen, *Chem Soc Rev*, 2017, **46**, 2824-2843.
50. J. S. Andersen, Y. W. Lam, A. K. L. Leung, S. E. Ong, C. E. Lyon, A. I. Lamond and M. Mann, *Nature*, 2005, **433**, 77-83.

51. D. Greuter, A. Loy, M. Horne and T. Ratteil, *Nucleic Acids Res*, 2016, **44**, D586-D589.
52. U. Scheer and R. Hock, *Curr Opin Cell Biol*, 1999, **11**, 385-390.
53. C. Cao, P. Wei, R. Li, Y. Zhong, X. Li, F. Xue, Y. Shi and T. Yi, *Acs Sensors*, 2019, **4**, 1409-1416.
54. X. J. Wang, Y. N. Wang, H. He, X. Chen, X. Sun, Y. W. Sun, G. J. Zhou, H. Xu and F. Huang, *J Mater Chem B*, 2016, **4**, 779-784.
55. Y. Y. Cheng, C. M. Li, R. Z. Mu, Y. F. Li, T. T. Xing, B. B. Chen and C. Z. Huang, *Anal Chem*, 2018, **90**, 11358-11365.
56. S. G. Sun, J. T. Wang, D. Z. Mu, J. Y. Wang, Y. M. Bao, B. Qiao and X. J. Peng, *Chemical Communications*, 2014, **50**, 9149-9152.
57. S. K. Sheet, B. Sen, K. Aguan and S. Khatua, *Dalton T*, 2018, **47**, 11477-11490.
58. E. J. New, *Acs Sensors*, 2016, **1**, 328-333.
59. Y. Liu, W. J. Zhang, Y. M. Sun, G. F. Song, F. Miao, F. Q. Guo, M. G. Tian, X. Q. Yu and J. Z. Sun, *Dyes and Pigments*, 2014, **103**, 191-201.
60. A. Pandith, R. G. Siddappa and Y. J. Seo, *Journal of Photochemistry and Photobiology C: Photochemistry Reviews*, 2019, **40**, 81-116.
61. N. Stevens, N. O'Connor, H. Vishwasrao, D. Samaroo, E. R. Kandel, D. L. Akins, C. M. Drain and N. J. Turro, *J Am Chem Soc*, 2008, **130**, 7182-7183.
62. Q. Li and Y.-T. Chang, *Nature Protocols*, 2006, **1**, 2922-2932.
63. Z. Li, S. Sun, Z. Yang, S. Zhang, H. Zhang, M. Hu, J. Cao, J. Wang, F. Liu, F. Song, J. Fan and X. Peng, *Biomaterials*, 2013, **34**, 6473-6481.
64. W. Liu, B. Zhou, G. Niu, J. Ge, J. Wu, H. Zhang, H. Xu and P. Wang, *ACS Applied Materials & Interfaces*, 2015, **7**, 7421-7427.
65. A. Saady, E. Varon, A. Jacob, Y. Shav-Tal and B. Fischer, *Dyes and Pigments*, 2020, **174**, 107986.
66. A. Cesaretti, E. Calzoni, N. Montegiove, T. Bianconi, M. Alebardi, M. A. La Serra, G. Consiglio, C. G. Fortuna, F. Elisei and A. Spalletti, *Journal*, 2023, **24**, 4812.
67. B. Shirinfar, N. Ahmed, Y. S. Park, G.-S. Cho, I. S. Youn, J.-K. Han, H. G. Nam and K. S. Kim, *Journal of the American Chemical Society*, 2013, **135**, 90-93.
68. Y.-J. Lu, Q. Deng, D.-P. Hu, Z.-Y. Wang, B.-H. Huang, Z.-Y. Du, Y.-X. Fang, W.-L. Wong, K. Zhang and C.-F. Chow, *Chemical Communications*, 2015, **51**, 15241-15244.
69. H. Li, Y. Li, H. Zhang, G. Xu, Y. Zhang, X. Liu, H. Zhou, X. Yang, X. Zhang and Y. Tian, *Chemical Communications*, 2017, **53**, 13245-13248.
70. G. Martini, E. Martinelli, G. Ruggeri, G. Galli and A. Pucci, *Dyes and Pigments*, 2015, **113**, 47-54.
71. V. Rathore, A. Upadhyay and S. Kumar, *Organic Letters*, 2018, **20**, 6274-6278.
72. S. Panda, A. Panda and S. S. Zade, *Coordination Chemistry Reviews*, 2015, **300**, 86-100.
73. P. Gaur, A. Kumar, G. Dey, R. Kumar, S. Bhattacharyya and S. Ghosh, *ACS Applied Materials & Interfaces*, 2016, **8**, 10690-10699.
74. P. Gaur, M. Galkin, A. Kurochka, S. Ghosh, D. A. Yushchenko and V. V. Shvadchak, *ACS Chemical Neuroscience*, 2021, **12**, 1293-1298.
75. K. Gavvala, S. Satpathi and P. Hazra, *RSC Advances*, 2015, **5**, 72793-72800.
76. K. Y. Law, *Chemical Physics Letters*, 1980, **75**, 545-549.
77. P. Ning, P. Dong, Q. Geng, L. Bai, Y. Ding, X. Tian, R. Shao, L. Li and X. Meng, *J Mater Chem B*, 2017, **5**, 2743-2749.
78. K. Maleckaitė, J. Dodonova, S. Toliautas, R. Žilėnaitė, D. Jurgutis, V. Karabanovas, S. Tumkevičius and A. Vyšniauskas, *Chemistry – A European Journal*, 2021, **27**, 16768-16775.
79. H. Xiao, P. Li and B. Tang, *Chemistry – A European Journal*, 2021, **27**, 6880-6898.
80. Y. Wu, C. Yin, W. Zhang, Y. Zhang and F. Huo, *Anal Chem*, 2022, **94**, 5069-5074.
81. S. Bicknese, N. Periasamy, S. B. Shohet and A. S. Verkman, *Biophysical Journal*, 1993, **65**, 1272-1282.